Improved Hydrogen Storage Kinetics of Nanoconfined $NaAlH_4$ Catalyzed with $TiCl_3$ Nanoparticles

Thomas K. Nielsen,[†] Marek Polanski,[‡] Dariusz Zasada,[‡] Payam Javadian,[†] Flemming Besenbacher,[§] Jerzy Bystrzycki,[‡] Jørgen Skibsted,[⊥] and Torben R. Jensen[†,*]

[†]Center for Energy Materials, Interdisciplinary Nanoscience Center (iNANO), and Department of Chemistry, Aarhus University, DK-8000 Aarhus, Denmark, [‡]Faculty of Advanced Technology and Chemistry, Military University of Technology, 2 Kaliskiego Str., 00-908 Warsaw, Poland, [§]Interdisciplinary Nanoscience Center (iNANO) and Department of Physics and Astronomy, Aarhus University, DK-8000 Aarhus C, Denmark, and [⊥]Instrument Centre for Solid-State NMR Spectroscopy, Department of Chemistry, and Interdisciplinary Nanoscience Center (iNANO), Aarhus University, DK-8000 Aarhus C, Denmark

ABSTRACT Nanoparticles of $NaAlH_4$ have been infiltrated in nanoporous carbon aerogel with $TiCl_3$ nanoparticles in order to explore possible synergetic effects between nanoconfinement and a functionalized catalytic scaffold. Resorcinol formaldehyde carbon aerogels with an average pore size of 17 nm and total pore volume of 1.26 mL/g were infiltrated with $TiCl_3$ to obtain an aerogel doped with 3.0 wt % $TiCl_3$ nanoparticles. $NaAlH_4$ was melt-infiltrated into the functionalized carbon aerogel at 189 °C and $p(H_2) \sim 186-199$ bar. Energy-dispersive spectrometry (EDS) combined with focused ion beam (FIB) techniques revealed the presence of Na, Al, Ti, and Cl inside the aerogel scaffold material. The infiltrated $NaAlH_4$ was X-ray amorphous, whereas ^{27}Al magic-angle spinning (MAS) NMR spectroscopy confirmed the presence of nanoconfined $NaAlH_4$. Temperature-programmed desorption mass spectroscopy (TPD-MS) and Sieverts' measurements demonstrated significantly improved hydrogen desorption kinetics for this new nanoconfined $NaAlH_4-TiCl_3$ material as compared to nanoconfined $NaAlH_4$ without the catalysts $TiCl_3$ and to bulk ball-milled samples of $NaAlH_4-TiCl_3$. We find that the onset temperature for hydrogen release was close to room temperature (T_{onset} = 33 °C), and the hydrogen release rate reached a maximum value at 125 °C, which demonstrates favorable synergetic effects between nanoconfinement and catalyst addition.

KEYWORDS: nanoconfinement · nanoporous · carbon aerogel · hydrogen storage · catalysis · sodium aluminum hydride

Increasing energy demands, the depletion of fossil fuels in the 21st century, and increasing levels of atmospheric carbon dioxide, which may induce global climate changes, call for a transition toward utilization of renewable and sustainable energy sources.[1,2] One of the major problems in a society based on sustainable energy sources, such as solar, wind, and water, where the temporal energy production varies significantly, is to develop a robust, efficient, inexpensive energy storage scheme. Hydrogen has indeed been suggested as a carrier of renewable energy in a future carbon-free energy system, but a requirement is that hydrogen can be stored with high gravimetric and volumetric density to reach sufficiently high energy capacities (*e.g.*, for mobile applications).[3,4] Furthermore, the kinetics of hydrogen release and uptake must be fast (~2 kg H_2/min) to obtain a short refueling time.[5,6] In addition, the thermodynamics of the hydrogen storage system should preferably be compatible with low-temperature proton exchange membrane (PEM) fuel cell technology and allow operation in the pressure and temperature range of $p(H_2) = 3-12$ bar and $T = -40$ to 85 °C, that is, corresponding to an enthalpy of formation, ΔH_f, in the range of −30 to −48 kJ/mol H_2.[3,5,6] To date, no material simultaneously fulfills all of the above-mentioned requirements.[4,7] Many conventional metals and alloys react with hydrogen gas, forming metal hydrides such as MgH_2 or complex metal hydrides such as $NaAlH_4$ and $LiBH_4$.[3] Sodium aluminum hydride, $NaAlH_4$, was one of the first complex hydrides to be considered due to suitable thermodynamic properties and high gravimetric and volumetric hydrogen content (7.5 wt % H_2 and 94 g H_2/L).[8] $NaAlH_4$ is known to release hydrogen in three steps according to reaction scheme 1:

$$3NaAlH_4(s) \leftrightarrow Na_3AlH_6(s) + 2Al(s) + 3H_2(g) \quad \text{(I)}$$

$$Na_3AlH_6(s) \leftrightarrow 3NaH(s) + Al(s) + 3/2H_2(g) \quad \text{(II)}$$

$$NaH(s) \leftrightarrow Na(l) + 1/2H_2(g) \quad \text{(III)}$$

The enthalpies for hydrogen release in steps I, II, and III are ΔH_D = 37, 47, and 56 kJ/mol H_2, respectively, corresponding to hydrogen release at T_{eq} = 30 and 100 °C ($p(H_2)$ = 1 bar) for steps I and II, respectively.[8,9] However, owing to kinetic limitations, decomposition only takes place at temperatures higher than $T > 180$

* Address correspondence to trj@chem.au.dk.

Received for review February 16, 2011 and accepted March 29, 2011.

Published online March 29, 2011
10.1021/nn200643b

and 240 °C for steps I and II, respectively. Hydrogen release from NaH, step III, takes place at temperatures above 425 °C and is usually not considered, that is, the practical hydrogen content of $NaAlH_4$ is 5.6 wt % H_2.[9,10] After the decomposition of $NaAlH_4$(s) into NaH(s) and Al(s), rehydrogenation requires high pressure and extended periods of time. However, improved hydrogen release and uptake kinetics can be obtained using catalytic additives such as Ti, Sc, or Ce, grain refinement, and homogenization by mechanical treatment (ball milling).[11−14]

Nanoconfinement is a new concept where nanoparticles of hydrides can be synthesized or melt-infiltrated into a nanoporous inert scaffold material where the metal hydride particle size is limited by the average pore size of the scaffold, allowing for the direct synthesis of small nanoparticles. The scheme of nanoconfinement has several advantages: (*i*) increased surface area of the reactants, (*ii*) nanoscale diffusion distances, and (*iii*) increased number of grain boundaries, which all facilitate the release and uptake of hydrogen and enhance the reaction kinetics.[15−18] Furthermore, particle growth and agglomeration of the nanoparticles may be hindered by the compartmentalization within the scaffold template. Nanoconfinement usually improves the kinetics and may also change the reaction mechanism and thereby the thermodynamics. The stability of nanoconfined chemical reactions may also be improved, that is, with preservation of the hydrogen storage capacity during cycling release and uptake of H_2. The design of new nanomaterials is expected to have a major impact on the development of novel sustainable energy and especially efficient energy storage technologies.[9,18−32]

Although, nanoconfinement of $NaAlH_4$ in both porous carbon and silica scaffolds mediates significantly improved hydrogen desorption kinetics and reversibility as compared to pristine $NaAlH_4$,[9,33] bulk $NaAlH_4$ ball-milled with $TiCl_3$ remains the superior system.[23] This has prompted the present investigation of the possible synergetic effects between nanoconfinement and catalytic additives for $NaAlH_4$ infiltrated in $TiCl_3$-functionalized carbon aerogels as a mean to further improve the hydrogen storage properties of $NaAlH_4$.

RESULTS AND DISCUSSION

Nanoporous Scaffold Materials. Nanoporous resorcinol formaldehyde carbon aerogel scaffold materials were synthesized for this study, and their texture parameters are given in Table 1. The pristine aerogel material, denoted X, has a BET surface area (S_{BET}) of 735 m^2/g, a total pore volume (V_{tot}) of 1.26 mL/g, and an average pore diameter (D_{max}) of 17 nm. These values are in good agreement with previous results for materials prepared under similar conditions.[19,20,34] Aerogel X was infiltrated with $TiCl_3$ dissolved in acetone to obtain functionalized aerogel monoliths doped with $TiCl_3$ nanoparticles (3.0 wt %). The uptake of $TiCl_3$ was determined from the weight gain of the aerogel and the sample is denoted Ti-X. Table 1 reveals that aerogels X and Ti-X have similar texture parameters; that is, the nanoporous network does not collapse due to infiltration with $TiCl_3$. However, the total pore volume and surface area of aerogel Ti-X is slightly reduced as compared to that of aerogel X, indicating the presence of $TiCl_3$ inside the pores. Bulk samples without aerogel of $NaAlH_4$ and $NaAlH_4$ with $TiCl_3$ (4 mol %) were prepared by ball milling and used as references. These samples are denoted Na-BM, Na-Ti-BM, and Na-Ti-BM-(II), respectively. Na-Ti-BM(II) was exposed to prolonged ball milling as compared to a Na-Ti-BM sample, and it was prepared to further study the effects of ball milling on the $NaAlH_4$-$TiCl_3$ system.

TABLE 1. Texture Parameters for the Pristine (X) and $TiCl_3$-Functionalized (Ti-X) Nanoporous Carbon Aerogel Scaffold Materials

RF aerogel	S_{BET} (m^2/g)	V_{meso} (mL/g)	V_{tot} (mL/g)	V_{micro}/V_{tot}	D_{max} (nm)
X	735	1.10	1.26	0.14	17
Ti-X	668	1.03	1.17	0.13	17

Sodium Aluminum Hydride Nanoparticles. The two aerogel samples X and Ti-X were separately and carefully grinded together with 33.3 wt % $NaAlH_4$. The amount of infiltrated $NaAlH_4$ is calculated from the bulk density of $NaAlH_4$ (ρ = 0.905 g/mL) and the total pore volumes of aerogels X and Ti-X (V_{tot}) to be 43 and 47 vol %, respectively, well below the saturation limit of the aerogel in order to obtain complete infiltration of $NaAlH_4$. Previous studies revealed that melt infiltration of higher amounts of $NaAlH_4$ into porous carbon (V_{tot} = 0.65 mL/g and D_{max} = 2−3 nm) leads to a composite material in which $NaAlH_4$ has both nano- and bulk-like properties.[9] $NaAlH_4$ was melt-infiltrated at T = 190 °C in a hydrogen atmosphere, $p(H_2) \sim 186-199$ bar for 10 h, in order to prevent decomposition of the hydride. The samples of $NaAlH_4$ nanoconfined in aerogels X and Ti-X are denoted Na-X and Na-Ti-X, respectively. The $NaAlH_4$ melt infiltration process was studied using *in situ* synchrotron radiation powder X-ray diffraction (SR-PXD),[35] and diagrams measured for sample Na-X before and after melt infiltration are shown in Figure 1a, b, respectively. Diffraction from $NaAlH_4$ is observed in both diagrams, although the diffracted intensity from melt-infiltrated $NaAlH_4$ is less intense, which may be due to partial decomposition of $NaAlH_4$. Full width at half-maximum values for Si, $NaAlH_4$, and Al Bragg peaks in Figure 1b are extracted using Rietveld refinements, and the crystallite sizes are calculated using the Scherrer formula and possible stress and strain is neglected (see the Supporting Information). The average crystallite size of $NaAlH_4$ is ∼34 nm, confirming the

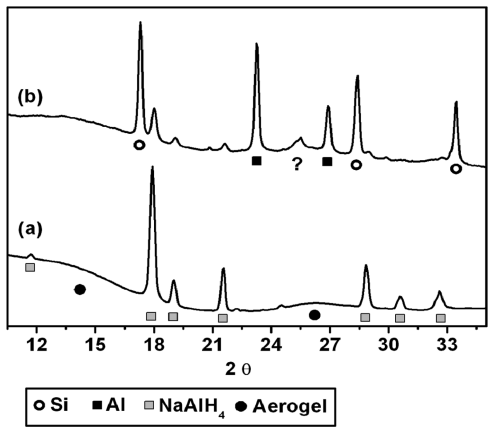

Figure 1. Synchrotron radiation powder X-ray diffraction diagrams measured at room temperature. (a) Mixture of $NaAlH_4$ and aerogel X. (b) $NaAlH_4$ melt-infiltrated in aerogel X (sample Na-X). Si PXD standard was added to this sample in order to estimate the instrumental Bragg peak broadening. The diagrams were normalized according to the most intense reflections from $NaAlH_4$ and Si (λ = 0.93813 Å).

formation of nanoparticles due to melt infiltration in aerogel X. This value is larger than the average pore size of aerogel X, D_{max} = 17 nm, derived by gas sorption measurements (Table 1) and may suggest that the melt infiltration approach facilitates crystallization of $NaAlH_4$ both in the small (≤17 nm) and the larger pores in the aerogel. The average crystallite size of aluminum is above 100 nm, indicating that Al resides on the surface of the aerogel. Partial decomposition of $NaAlH_4$ and formation of Al during melt infiltration at elevated hydrogen pressure is consistent with previous studies.[9,23,36] Broad reflections at $2\theta \sim 14.3$ and 26.3° are observed in both diagrams due to the graphite-like structural features within the aerogel material, in agreement with previous studies.[19,20,37]

The powder X-ray diffraction pattern for sample Na-Ti-X contains no diffraction from melt-infiltrated $NaAlH_4$, indicating that it is either X-ray amorphous or fully decomposed (Figure S3 in Supporting Information). Energy-dispersive spectrometry (EDS) and ^{27}Al MAS NMR spectroscopy are utilized to verify the presence of $NaAlH_4$ and $TiCl_3$ inside aerogel Ti-X after melt infiltration. Furthermore, focused ion beam (FIB) techniques allow studying the interior of sample Na-Ti-X by EDS elemental analysis (Figures S1 and S2 in Supporting Information). The analysis reveals the presence of carbon, oxygen, sodium, aluminum, chloride, and titanium inside the aerogel material. Carbon and oxygen are part of the aerogel structure,[38] but oxygen may also originate from partial oxidation of aluminum due to the exposure to ambient conditions prior to the X-ray analysis. For comparison, sample Na-X was also subjected to this analysis, revealing Na and Al inside the scaffold material. These FIB-EDS results confirm that sodium, aluminum, and titanium catalyst are successfully nanoconfined in the aerogel (see

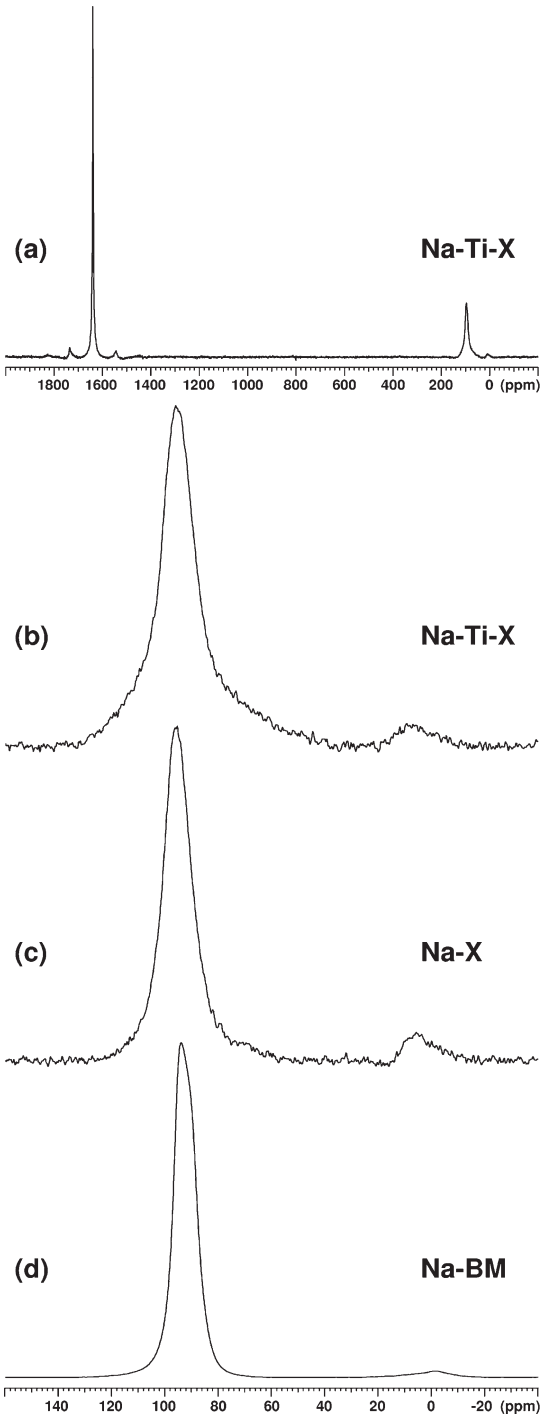

Figure 2. ^{27}Al MAS NMR spectra (9.4 T) illustrating the central transition region for the AlH_4^- units in (b) melt-infiltrated $NaAlH_4$ in aerogel Ti-X (sample Na-Ti-X), (c) melt-infiltrated $NaAlH_4$ in aerogel X (sample Na-X), and (d) ball-milled $NaAlH_4$ (sample Na-BM). The full spectrum, including the central transition for metallic Al(s) and employing a transmitter offset of 800 ppm, is illustrated (a) for sample Na-Ti-X.

Figure S2 in the Supporting Information). Samples Na-Ti-X, Na-X, and Na-BM were subsequently studied using ^{27}Al MAS NMR spectroscopy (Figure 2).

The ^{27}Al MAS NMR spectrum of the ball-milled sample, Na-BM (Figure 2d), shows a central transition

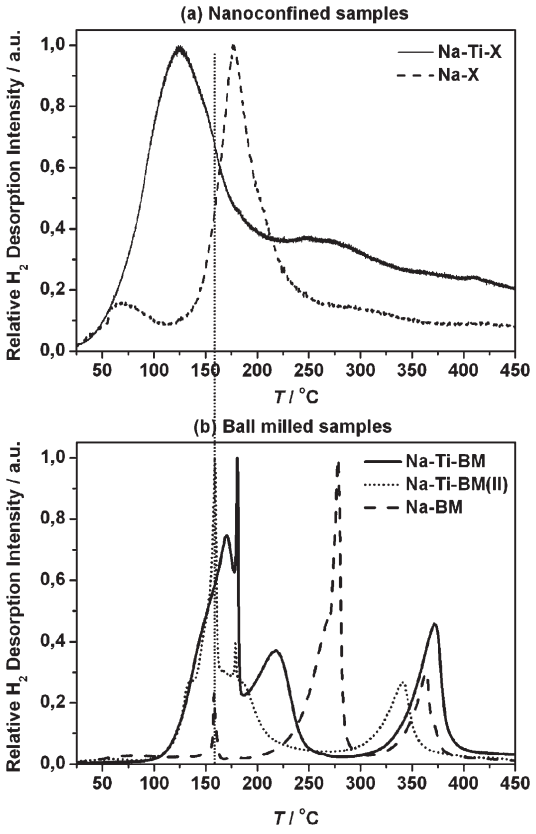

Figure 3. Normalized TPD-MS profiles measured from room temperature to 450 °C (heating rate 5 °C/min) by recording the mass spectrometer intensity of H_2^+ ions (m/e = 2). (a) Relative hydrogen desorption intensities for the two nanoconfined samples, Na-Ti-X and Na-X. (b) Relative hydrogen desorption intensities for the ball-milled samples, Na-Ti-BM, Na-Ti-BM(II), and Na-BM.

resonance from $NaAlH_4$ with a center of gravity at 92.7 ppm in accordance with the ^{27}Al chemical shift and quadrupole coupling reported earlier for this compound.[9,24,39] In addition to the resonance from $NaAlH_4$, the Na-Ti-X and Na-X samples also include a resonance from metallic Al(s) at 1639.5 ppm,[40] as illustrated in Figure 2a for the Na-Ti-X sample, and a small resonance at 8 ppm. The latter peak is ascribed to a less crystalline/amorphous impurity phase including AlO_6^{9-} octahedra. Noteworthy, the ^{27}Al NMR spectra of the Na-X and Na-Ti-X samples show the absence of Na_3AlH_6, demonstrating that the fraction of $NaAlH_4$ that is lost during melt infiltration is fully decomposed to Al and presumably NaH. The center of gravity for the central transition from $NaAlH_4$ in the ^{27}Al MAS NMR spectra is observed at 94.6, 96.9, and 92.7 ppm for the samples Na-Ti-X, Na-X, and Na-BM, respectively, while the corresponding line widths (fwhm) are 14.5, 11.9, and 9.2 ppm. The slight increase in chemical shift and line broadening has previously been observed for nanoconfined $NaAlH_4$ in mesoporous carbon where these effects were ascribed to a higher degree of disorder for the Al environment in $NaAlH_4$ caused by the close contact with the scaffold material.[9,24] The fact

TABLE 2. Temperature for the Onset of Hydrogen Release, T_{onset}, and the Maximum of the Relative Hydrogen Desorption Intensity, T_{max}, for the Major Hydrogen Release Peaks

sample	T_{onset}/°C	T_{max}/°C[b]
Na-BM	200	278
Na-X	125	176
Na-Ti-BM	100	170–180
Na-Ti-BM(II)	100	159
Na-Ti-X	33	125
equilibrium temp[a]	30	100

[a] The calculated equilibrium temperatures for hydrogen release from $NaAlH_4$ using thermodynamic data for reactions I and II, respectively. [b] Measured value for the major hydrogen release peak.

that $NaAlH_4$ in the $TiCl_3$-doped aerogel is X-ray amorphous and shows more substantial line broadening effects in the ^{27}Al MAS NMR spectrum indicates that the presence of $TiCl_3$ nanoparticles mediates the formation of a highly disordered nanoconfined material.

Kinetic Properties of the Nanoconfined $NaAlH_4$. The hydrogen desorption kinetics of the first desorption cycle for samples Na-Ti-X, Na-X, Na-BM, Na-Ti-BM, and Na-Ti-BM(II) are studied using simultaneous temperature-programmed desorption and mass spectroscopy, TPD-MS (Figure 3). The characteristic parameters extracted from these studies are the onset temperature, T_{onset}, for the release of hydrogen and the temperature, T_{max}, where the relative hydrogen desorption intensity reaches its maximum value. Furthermore, the appearance of several maxima on the desorption curve suggests several desorption processes with different reaction rates; that is, the shape of the curve may be used to distinguish nanoconfined and bulk properties of the samples.

The characteristic values T_{onset} and T_{max} are extracted from Figure 3 and listed in Table 2. These data demonstrate that hydrogen desorption occurs at lower temperatures for nanoconfined $NaAlH_4$ as compared to ball-milled $NaAlH_4$; however, ball milling $NaAlH_4$ with $TiCl_3$ mediates even faster kinetics. It should be noted that sample Na-Ti-BM(II) was ball-milled under considerably more severe conditions than sample Na-Ti-BM, which reduces the T_{max} value from 170–180 to 159 °C, while the onset temperature for hydrogen release remains unchanged, T_{onset} = 100 °C. The T_{max} value of 176 °C for sample Na-X agrees well with previous studies of melt-infiltrated $NaAlH_4$ in mesoporous materials.[9,23,33] Sample Na-Ti-X has T_{onset} and T_{max} values of 33 and 125 °C, respectively, showing that nanoconfinement of $NaAlH_4$ in aerogel doped with $TiCl_3$ nanoparticles mediates significantly improved hydrogen desorption kinetics as compared to nanoconfined $NaAlH_4$ without $TiCl_3$. This is evident from the significant reduction of the T_{onset} and T_{max} values, which have been reduced by 92 and 51 °C, respectively. Furthermore, combining nanoconfinement of

$NaAlH_4$ with catalytically active $TiCl_3$ (Na-Ti-X) nanoparticles in a functionalized carbon aerogel mediates higher relative hydrogen desorption intensities as compared to ball milling $NaAlH_4$ with $TiCl_3$ (Na-Ti-BM-(II)) since $\Delta T_{onset} \sim -77$ °C and $\Delta T_{max} \sim -34$ °C, indicating a favorable synergetic effect between nanoconfinement and catalytic $TiCl_3$ nanoparticles.

It is noteworthy, that the hydrogen release temperatures from sample Na-Ti-X are similar to the equilibrium temperatures $T_{eq} = 30$ and 100 °C for reaction steps I and II, respectively, calculated from the thermodynamic data for $NaAlH_4$. Samples Na-BM, Na-Ti-BM, and Na-Ti-BM(II) have local T_{max} values at 363, 372, and 341 °C, respectively, due to the decomposition of NaH(s) forming Na(l). For the nanoconfined samples, this local maximum is less evident due to nanoconfinement of NaH, in accordance with previous studies.[9,41] Samples Na-X and Na-BM have local T_{max} at 54 and 158 °C, respectively, which only appears when the experiment is carried out in a graphite crucible (see the Supporting Information).

Cyclic Stability, Reversibility, and Kinetics. The reversible hydrogen storage capacity and desorption kinetics for nanoconfined and ball-milled $NaAlH_4$ were studied by Sieverts' method. A total of four hydrogen release and uptake cycles were measured, and the desorption profiles are depicted in Figure 4. Since previous studies reveal that pristine $NaAlH_4$ cannot be cycled with hydrogen at moderate conditions, sample Na-BM was not investigated.[9,23]

The nanoconfined $NaAlH_4$ in the $TiCl_3$-functionalized aerogel (Na-Ti-X) releases 2.9 wt % H_2/$NaAlH_4$ during the first desorption (corresponding to 0.97 wt % H_2 relative to the mass of the sample). The second, third, and fourth hydrogen desorption cycles release 2.0, 1.8, and 1.6 wt % H_2/$NaAlH_4$, respectively. All hydrogen absorptions were carried out at 160 °C and $p(H_2) = 100$ bar during 10 h. The nanoconfined sample Na-X releases 3.1 wt % H_2/$NaAlH_4$ during the first desorption cycle (corresponding to 1.0 wt % H_2/sample). The second, third, and fourth desorption cycles release 2.3, 2.0, and 1.7 wt % H_2/$NaAlH_4$ respectively; that is, nanoconfined $NaAlH_4$ shows reasonable cyclic stability, which can be further optimized in accordance with previous studies.[9]

During the first desorption, samples Na-Ti-X and Na-X release 2.9 and 3.1 wt % H_2/$NaAlH_4$, respectively, which is lower than the expected value of 5.6 wt % H_2/$NaAlH_4$ for reaction steps I and II. These results indicate that ~52 and 55% of the added $NaAlH_4$ is successfully melt-infiltrated into aerogels Ti-X and X, respectively, while the remaining fraction apparently decompose, forming Al(s) and NaH(s). The amount of infiltrated $NaAlH_4$ in sample Na-Ti-X is expected to be lowered due to irreversible reactions between molten $NaAlH_4$ and $TiCl_3$, forming NaCl and Al_xTi_y.[42,43] In fact, the reduction in hydrogen capacity from 3.1 to 2.9 wt % H_2/$NaAlH_4$ compares with the amount of $TiCl_3$ (3.0 wt %) incorporated in aerogel Ti-X (calculated value assuming full reduction of Ti^{3+} to Ti, 2.7 wt % H_2/$NaAlH_4$). The relative amounts of Al(s) and $NaAlH_4$(s) can also be estimated from the ^{27}Al MAS NMR spectra, employing the same approach as used in an earlier study of a mixture of Al(s) and $LiAlH_4$.[40] This method gives the presence of 64 ± 5 and 43 ± 5 mol % $NaAlH_4$ in the Na-Ti-X and Na-X samples, respectively, which is in accord with the remaining hydrogen storage capacity content calculated from the Sieverts data (*i.e.*, ~52 and 55% $NaAlH_4$, respectively).

The sample of $NaAlH_4$ ball-milled with $TiCl_3$ (Na-Ti-BM) releases 5.1 wt % H_2/$NaAlH_4$ during the first

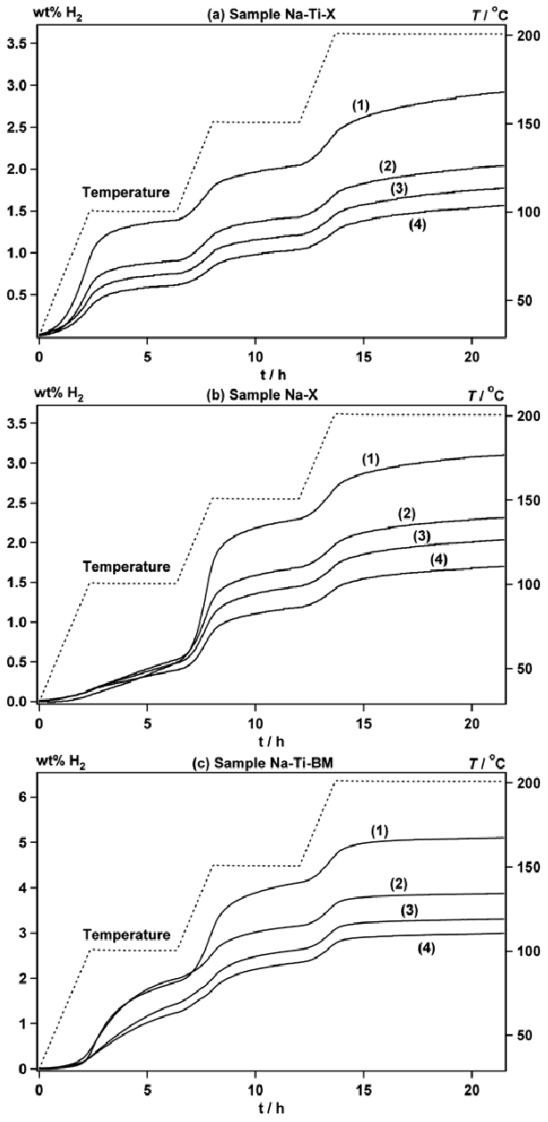

Figure 4. Sieverts' measurements showing hydrogen desorption cycles 1 to 4 for samples (a) Na−Ti-X, (b) Na-X, and (c) Na-Ti-BM. Melt infiltration of $NaAlH_4$ into aerogels Ti-X and X was performed prior to the first desorption cycle to obtain samples Na-Ti-X and Na-X, respectively. Hydrogen desorption was performed at fixed temperatures of 100, 150, and 200 °C (heating rate 0.5 °C/min; see the dashed lines). Hydrogen absorption was carried out at 160 °C and $p(H_2) = 100$ bar during 10 h.

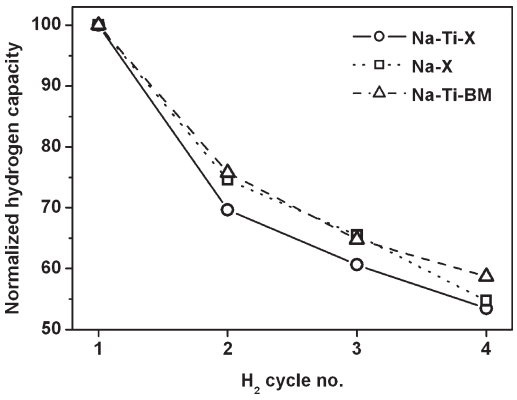

Figure 5. Normalized cyclic hydrogen storage capacities for samples Na-Ti-X (circles, solid line), Na-X (squares, dotted line), and Na-Ti-BM (triangles, dashed line). The lines are plotted as a guide to the eye. Samples were hydrogenated at 160 °C and $p(H_2) \sim 110$ bar during 10 h between each desorption.

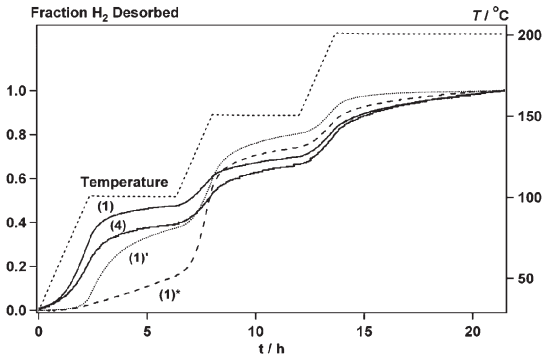

Figure 6. Normalized Sieverts' hydrogen desorption profiles (data from Figure 4a–c). The hydrogen release kinetics for samples Na-Ti-X (solid lines) cycles 1 and 4, Na-X (dashed line), and Na-Ti-BM (dotted line) are compared.

desorption cycle; that is, 91% of the full hydrogen capacity (5.6 wt % H_2) is released. Assuming that $NaAlH_4$ reacts with $TiCl_3$ during ball milling in the ratio of 3:1 leads to a calculated hydrogen content of 4.9 wt % for sample Na-Ti-BM. The second, third, and fourth hydrogen desorption cycles release 3.9, 3.3, and 3.0 wt % $H_2/NaAlH_4$, respectively. The reversible hydrogen storage capacity during four hydrogen release and uptake cycles for the samples Na-Ti-X, Na-X, and Na-Ti-BM is compared in Figure 5.

Sample Na-Ti-X releases 70, 61, and 54% of the initial hydrogen content during desorption cycles 2, 3, and 4, respectively, while sample Na-X releases 75, 66, and 55%. Sample Na-Ti-BM released 76, 65, and 59% during desorption cycles 2, 3, and 4, respectively. The stability of the three samples during cycling hydrogen release and uptake seems to be similar, although the ball-milled samples have a slightly higher preserved capacity. The physical conditions for hydrogen uptake may be further optimized to achieve faster and more complete absorption, for example, by choosing a lower final desorption temperature below the melting point of $NaAlH_4$, which may limit the irreversible formation of Al(s) agglomerates.[44]

In Figure 6, the kinetic properties of the nanoconfined and ball-milled samples are compared based on the normalized hydrogen desorption profiles.

Sample Na-Ti-X has a significantly faster hydrogen relative desorption intensity at lower temperatures and releases 32% of the hydrogen content during heating to $T < 100$ °C within 2.38 h, while samples Na-Ti-BM and Na-X only release 6 and 3%, respectively. Furthermore, samples Na-Ti-X, Na-Ti-BM, and Na-X release 48, 38 and 16% of the hydrogen content below $T \leq 100$ °C during 6.32 h. These findings show that the hydrogen desorption kinetics are improved considerably by nanoconfinement of $NaAlH_4$ in $TiCl_3$-functionalized aerogel as compared to a ball-milled $NaAlH_4$-$TiCl_3$ sample. In contrast, sample Na-X has the faster relative desorption intensity at $T \geq 150$ °C. The fourth normalized hydrogen desorption profile for sample Na-Ti-X is also plotted in Figure 6 and shows a fast relative desorption intensity at low temperatures (*i.e.*, preserved synergetic effects).

Samples Na-Ti-X and Na-X both released ~3 wt % $H_2/NaAlH_4$ during the first desorption (Figure 5a,b), corresponding to ~1 wt % H_2 relative to the mass of storage material. This low value for the gravimetric hydrogen content of the nanocomposite materials can be optimized in several ways. Decomposition of $NaAlH_4$ during infiltration may be suppressed using higher hydrogen pressure and possibly shorter infiltration time. The loading of $NaAlH_4$ into the nanoporous material may be optimized by several repetitive infiltration cycles. The infiltrated $NaAlH_4$ occupies <47% of the available pore volume in the aerogel scaffold in sample Na-Ti-X. Furthermore, the total pore volume of the scaffold material may also be optimized, for example, by employing super critical drying of the aerogels.[38,45]

The fact that $NaAlH_4$ embedded in $TiCl_3$-doped aerogel is X-ray amorphous and shows broadening of the ^{27}Al MAS NMR central transition indicates significant degree of disorder which may contribute to the improved hydrogen desorption kinetics. A full understanding of the favorable synergetic effects observed between nanoconfinement and the catalytic $TiCl_3$-functionalized scaffold may hold the key to further improve the hydrogen release and uptake kinetics for $NaAlH_4$.

CONCLUSIONS

A new nanocomposite material of $NaAlH_4$ melt-infiltrated into nanoporous carbon aerogels functionalized with 3.0 wt % $TiCl_3$ catalytically active nanoparticles has been investigated. The hydrogen release rate from this material is significantly improved as compared to bulk $NaAlH_4$ ball-milled with $TiCl_3$ or $NaAlH_4$ nanoconfined in aerogel without $TiCl_3$. Thus, favorable synergetic effects between nanoconfinement and

utilization of a catalytic scaffold have been demonstrated. A full understanding of these synergetic effects may help to considerably improve hydrogen release and uptake kinetics for $NaAlH_4$. The combination of nanoconfinement and functionalized nanoporous scaffolds may develop to become an important scheme within the emerging area of nanotechnology for improving properties of a variety functional nanomaterials.

METHODS

Sample Preparations. The resorcinol formaldehyde aerogels, denoted X, were prepared by mixing 10.3476 g of resorcinol (Aldrich, 99%), 14.2 mL of a 37 wt % formaldehyde in water solution stabilized by ~10% methanol (Merck), 14.2 mL of deionized water, and 0.0610 g of Na_2CO_3 (Aldrich, 99.999%) in a beaker with continuous stirring. Afterward, the preparation and characterization was performed according to previously published procedures.[19,20,34]

A new procedure was developed to incorporate $TiCl_3$ into the aerogel material. Aerogel X was first activated at 400 °C in vacuum for several hours in order to remove moisture and gases from the porous structure. Afterward, 0.7104 g of aerogel monoliths was submerged into a solution of 0.0406 g of $TiCl_3$ (5.4 wt %, Aldrich, 99.995%) in 30 mL of dry acetone (Aldrich, ≥ 99.9%). This infiltration procedure was performed in a purified argon atmosphere in a glovebox. The aerogels in $TiCl_3$ were left to dry for several days until the solvent acetone was fully evaporated and $TiCl_3$ had crystallized in the pores. Afterward, the sample was activated at 375 °C in vacuum for 12 h. The final mass of the $TiCl_3$-doped aerogel, denoted Ti-X, was 0.7324 g; that is, the aerogel incorporated 3.0 wt % $TiCl_3$. A mixture of 34.2 mg of Na-X and 3.5 mg of Si (standard reference material NBS 640a with a mean crystallite size of 2 μm) was carefully ground and used for SR-PXD studies; see below.

Samples of aerogels X and Ti-X loaded with $NaAlH_4$ were prepared by grinding monoliths of aerogel together with $NaAlH_4$ (Aldrich, 90%), obtaining a powder. $NaAlH_4$ melts and starts to decompose to solid Na_3AlH_6 and Al at $T_{mp} \sim 183$ °C. Elevated hydrogen pressure can suppress decomposition, while molten $NaAlH_4$ infiltrates the nanoporous scaffold and nanoparticles are formed upon subsequent cooling.[9,23,24] Melt infiltration was performed under inert conditions in a PCTpro 2000 apparatus from Hy-Energy by applying a hydrogen pressure of 170−178 bar and heating to a temperature of 189 to 190 °C, reaching pressures in the range of 186−199 bar (heating rate 5 °C/min). The sample temperature was kept fixed at 189 °C for 10 h, and then the sample was cooled to 160 °C, reaching a pressure of 181−191 bar (cooling rate 20 °C/min), and after 7 h, the sample was cooled naturally to room temperature.

Three samples of ball-milled $NaAlH_4$ (without aerogel) were also prepared and used as references. A mixture of $NaAlH_4$ and $TiCl_3$ (4 mol %, 11 wt %) was placed in a wolfram carbide vial with 14 wolfram carbide balls (10 mm o.d.). Sodium aluminum hydride was added to a second vial also containing 14 wolfram carbide balls. Both vials were transferred to a Fritsch Pulverisette 4 and ball-milled for 1 h at 350 rpm (the ball to sample mass ratio was 108:1), and the samples are denoted Na-Ti-BM(II) and Na-BM, respectively. In addition, a mixture of $NaAlH_4$ and $TiCl_3$ (4 mol %, 11 wt %) was placed in a wolfram carbide vial with 7 wolfram carbide balls (10 mm o.d.; the ball to sample mass ratio was 49:1), transferred to a Fritsch Pulverisette 4 and ball-milled for 20 min at 400 rpm and is denoted Na-Ti-BM. All handling of samples was performed under a purified argon atmosphere in a glovebox.

SR-PXD Measurements. Synchrotron radiation powder X-ray diffraction (SR-PXD) data were collected at beamline I711 at MAX-lab, Lund, Sweden. A *ca.* 10 mm long powder sample was mounted in a sapphire capillary tube with an inner diameter of 0.79 mm and placed in an airtight sample holder at inert conditions in an argon-filled glovebox.[35] The sample holder was moved from the glovebox to the diffractometer without exposing the sample to air. The selected X-ray wavelength was $\lambda = 0.93813$ Å, and data were collected using a CCD detector.

Sieverts' Measurements. The cyclic stability of the samples Na-Ti-X, Na-X, and Na-Ti-BM was studied by Sieverts' measurements (PCTpro 2000) of four hydrogen release and uptake cycles. The samples were transferred to an autoclave and sealed under argon in a glovebox. The quantity of $NaAlH_4$ was in the range of 48 to 115 mg. The autoclave was attached to the PCTpro 2000 apparatus, and melt infiltration of $NaAlH_4$ was performed under the conditions described above. Hydrogen desorption data were collected in the temperature range from room temperature to 200 °C and with the temperature kept fixed at 100 °C for 4 h, at 150 °C for 4 h, and at 200 °C for 8 h (0.5 °C/min). Hydrogen absorption was performed at $p(H_2) = 100-104$ bar and at a temperature of 160 °C during 10 h, and the sample was cooled to room temperature naturally. The heating rate was 5 °C/min, and the pressure reached 108−112 bar at the final temperature.

^{27}Al MAS NMR. Solid-state ^{27}Al MAS NMR spectra were recorded on a Varian INOVA-400 (9.39 T) spectrometer, using a home-built X-[^{1}H] double-resonance MAS NMR probe for 5 mm o.d. rotors. The NMR experiments were performed at ambient temperatures and employed airtight end-capped zirconia rotors packed with the sample in an argon-filled glovebox. The ^{27}Al isotropic chemical shifts are in parts per million relative to a 1.0 M aqueous solution of $AlCl_3 \cdot 6H_2O$.

TPD-MS. Temperature-programmed desorption profiles were performed using a Setaram Sensys Evo differential scanning calorimeter (horizontal position) coupled with a quadrupole mass spectrometer (MS) under a constant flow (23 mL/min) of high purity argon (99.999% Air Liquide) or helium (99.9999% Air Liquide). Up to 20 mg of powdered sample was placed in a graphite crucible. The graphite crucible containing the sample was then encapsulated in a protective aluminum crucible. Loading of the samples was performed with no air contact. The samples were purged with argon and heated in the temperature range of 30−450 °C (heating rate 5 °C/min). During the experiment, the MS signals at $m/e = 2$, 18, and 32 were recorded in order to detect H_2, H_2O and O_2.

FIB-SEM-EDS. The morphology of nanoconfined $NaAlH_4$ with and without $TiCl_3$ was examined with an FEI Quanta 3D dual-beam field emission scanning electron microscope (SEM), equipped with a tungsten hairpin electron source and a gallium ion source (FIB) as well as an energy-dispersive X-ray spectrometer (EDS).

Acknowledgment. The work was supported by the Danish National Research Foundation (Centre for Materials Crystallography) and the Danish Strategic Research Council (Centre for Energy Materials). The Danish Council for Independent Research, Natural Sciences (FNU) is acknowledged for equipment grants. The access to beam time at the MAX-II synchrotron (Lund, Sweden) in the research laboratory MAX-lab is gratefully acknowledged. We are grateful to the Carlsberg Foundation and the Danish Natural Science Research Councils, for fundings to the Instrument Centre for Solid-State NMR Spectroscopy, and to the Polish Ministry of Science and Higher Education (Key Project POIG.01.03.01-14-016/08 and POIG.02.01.00-14-071/08/00).

Supporting Information Available: Crystallite size calculation using Rietveld refinements and the Scherrer formula, SR-PXD diagrams, scanning electron microscopy (SEM) images, energy-dispersive spectrometry (EDS), and additional TPD-MS data. This material is available free of charge *via* the Internet at http://pubs.acs.org.

REFERENCES AND NOTES

1. Liu, C. J.; Burghaus, U.; Besenbacher, F.; Wang, Z. L. Preparation and Characterization of Nanomaterials for Sustainable Energy Production. *ACS Nano* **2010,** *4*, 5517–5526.
2. Lewis, N. S.; Nocera, D. G. Powering the Planet: Chemical Challenges in Solar Energy Utilization. *Proc. Natl. Acad. Sci. U.S.A.* **2006,** *103*, 15729–15735.
3. Schlapbach, L.; Züttel, A. Hydrogen-Storage Materials for Mobile Applications. *Nature* **2001,** *414*, 353–358.
4. Eberle, U.; Felderhoff, M.; Schüth, F. Chemical and Physical Solutions for Hydrogen Storage. *Angew. Chem., Int. Ed.* **2009,** *48*, 6608–6630.
5. U.S. Department of Energy https://www1.eere.energy.gov/hydrogenandfuelcells/storage/pdfs/targets_onboard_hydro_storage.pdf.
6. U.S. Department of Energy https://www.eecbg.energy.gov/hydrogenandfuelcells/storage/pdfs/targets_onboard_hydro_storage_explanation.pdf.
7. Graetz, J. New Approaches to Hydrogen Storage. *Chem. Soc. Rev.* **2009,** *38*, 73–82.
8. Bogdanovic, B.; Brand, R. A.; Marjanovic, A.; Schwickardi, M.; Tölle, J. Metal-Doped Sodium Aluminium Hydrides as Potential New Hydrogen Storage Materials. *J. Alloys Compd.* **2000,** *302*, 36–58.
9. Gao, J.; Adelhem, P.; Verkuijlen, M. H. W.; Rongeat, C.; Herric, M.; van Bentum, P. J. M.; Gutfleisch, O.; Kentgens, A. P. M.; de Jong, K. P.; de Jongh, P. E. Confinement of $NaAlH_4$ in Nanoporous Carbon: Impact on H_2 Release, Reversibility, and Thermodynamics. *J. Phys. Chem. C* **2010,** *114*, 4675–4682.
10. Sakintuna, B.; Lamari-Darkrim, F.; Hirscher, M. Metal Hydride Materials for Solid Hydrogen Storage: A Review. *Int. J. Hydrogen Energy* **2007,** *32*, 1121–1140.
11. Sandrock, G.; Gross, K.; Thomas, G. Effect of Ti-Catalyst Content on the Reversible Hydrogen Storage Properties of the Sodium Alanates. *J. Alloys Compd.* **2002,** *339*, 299–308.
12. Bogdanovic, B.; Schwickardi, M. Ti-Doped $NaAlH_4$ as a Hydrogen-Storage Material—Preparation by Ti-Catalyzed Hydrogenation of Aluminum Powder in Conjunction with Sodium Hydride. *Appl. Phys. A: Mater. Sci. Process.* **2001,** *72*, 221–223.
13. Rongeat, C.; Jansa, I. L.; Oswald, S.; Schultz, L.; Gutfleisch, O. Mechanochemical Synthesis and XPS Analysis of Sodium Alanate with Different Additives. *Acta Mater.* **2009,** *57*, 5563–5570.
14. Bogdanovic, B.; Schwickardi, M. Ti-Doped Alkali Metal Aluminium Hydrides as Potential Novel Reversible Hydrogen Storage Materials. *J. Alloys Compd.* **1997,** *253–254*, 1–9.
15. Bérubé, V.; Radtke, G.; Dresselhaus, M.; Chen, G. Size Effects on the Hydrogen Storage Properties of Nanostructured Metal Hydrides: A Review. *Int. J. Energy Res.* **2007,** *31*, 637–663.
16. Zaluski, L.; Zaluska, A.; Ström-Olsen, J. O. Nanocrystalline Metal Hydrides. *J. Alloys Compd.* **1997,** *253–254*, 70–79.
17. Kirchheim, R.; Mütschele, T.; Kieninger, W.; Gleiter, H.; Birringer, R.; Koblé, T. D. Hydrogen in Amorphous and Nanocrystalline Metals. *Mater. Sci. Eng.* **1988,** *99*, 457–462.
18. Mueller, T.; Ceder, G. Effect of Particle Size on Hydrogen Release from Sodium Alanate Nanoparticles. *ACS Nano* **2010,** *4*, 5647–5656.
19. Nielsen, T. K.; Bösenberg, U.; Gosalawit, R.; Dornheim, M.; Cerenius, Y.; Besenbacher, F.; Jensen, T. R. A Reversible Nanoconfined Chemical Reaction. *ACS Nano* **2010,** *4*, 3903–3908.
20. Nielsen, T. K.; Manickam, K.; Hirscher, M.; Besenbacher, F.; Jensen, T. R. Confinement of MgH_2 Nanoclusters within Nanoporous Aerogel Scaffold Materials. *ACS Nano* **2009,** *3*, 3521–3528.
21. Gutowska, A.; Li, L. Y.; Shin, Y. S.; Wang, C. M. M.; Li, X. H. S.; Linehan, J. C.; Smith, R. S.; Kay, B. D.; Schmid, B.; Shaw, W.; *et al.* Nanoscaffold Mediates Hydrogen Release and the Reactivity of Ammonia Borane. *Angew. Chem., Int. Ed.* **2005,** *44*, 3578–3582.
22. Nielsen, T. K.; Besenbacher, F.; Jensen, T. R. Nanoconfined Hydrides for Energy Storage. *Nanoscale* 2011, DOI: 10.1039/C0NR00725K.
23. Stephens, R. D.; Gross, A. F.; Atta, S. L. V.; Vajo, J. J.; Pinkerton, F. E. The Kinetic Enhancement of Hydrogen Cycling in $NaAlH_4$ by Melt Infusion into Nanoporous Carbon Aerogel. *Nanotechnology* **2009,** *20*, 204018.
24. Verkuijlen, M. H. W.; Gao, J.; Adelhelm, P.; van Bentum, P. J. M.; de Jongh, P. E.; Kentgens, A. P. M. Solid-State NMR Studies of the Local Structure of $NaAlH_4$/C Nanocomposites at Different Stages of Hydrogen Desorption and Rehydrogenation. *J. Phys. Chem. C* **2010,** *114*, 4683–4692.
25. Gross, A. F.; Vajo, J. J.; Atta, S. L. V.; Olson, G. L. Enhanced Hydrogen Storage Kinetics of $LiBH_4$ in Nanoporous Carbon Scaffolds. *J. Phys. Chem. C* **2008,** *112*, 5651–5657.
26. Kim, H.; Karkamkar, A.; Autrey, T.; Chupas, P.; Proffen, T. Determination of Structure and Phase Transition of Light Element Nanocomposites in Mesoporous Silica: Case Study of NH_3BH_3 in MCM-41. *J. Am. Chem. Soc.* **2009,** *131*, 13749–55.
27. Paolone, A.; Palumbo, O.; Rispoli, P.; Cantelli, R.; Autrey, T.; Karkamkar, A. Absence of the Structural Phase Transition in Ammonia Borane Dispersed in Mesoporous Silica: Evidence of Novel Thermodynamic Properties. *J. Phys. Chem. C* **2009,** *113*, 10319–10321.
28. Berseth, P. A.; Harter, A. G.; Zidan, R.; Blomqvist, A.; Araújo, C. M.; Scheicher, R. H.; Ahuja, R.; Jena, P. Carbon Nanomaterials as Catalysts for Hydrogen Uptake and Release in $NaAlH_4$. *Nano Lett.* **2009,** *9*, 1501–1505.
29. Wellons, M. S.; Berseth, P. A.; Zidan, R. Novel Catalytic Effects of Fullerene for $LiBH_4$ Hydrogen Uptake and Release. *Nanotechnology* **2009,** *20*, 204022.
30. de Jongh, P. E.; Adelhelm, P. Nanosizing and Nanoconfinement: New Strategies towards Meeting Hydrogen Storage Goals. *ChemSusChem* **2010,** *3*, 1332–1348.
31. Lohstroh, W.; Roth, A.; Hahn, H.; Fichtner, M. Thermodynamic Effects in Nanoscale $NaAlH_4$. *ChemPhysChem* **2010,** *11*, 789–792.
32. Zhao-Karger, Z.; Hu, J.; Roth, A.; Wang, D.; Kubel, C.; Lohstroh, W.; Fichtner, M. Altered Thermodynamic and Kinetic Properties of MgH_2 Infiltrated in Microporous Scaffold. *Chem. Commum.* **2010,** *46*, 8353–8355.
33. Zheng, S.; Fang, F.; Zhou, G.; Chen, G.; Ouyang, L.; Zhu, M.; Sun, D. Hydrogen Storage Properties of Space-Confined $NaAlH_4$ Nanoparticles in Ordered Mesoporous Silica. *Chem. Mater.* **2008,** *20*, 3954–3958.
34. Li, W.-C.; Lu, A.-H.; Weidenthaler, C.; Schüth, F. Hard-Templating Pathway To Create Mesoporous Magnesium Oxide. *Chem. Mater.* **2004,** *16*, 5676–5681.
35. Jensen, T. R.; Nielsen, T. K.; Filinchuk, Y.; Jørgensen, J.-E.; Cerenius, Y.; Gray, E. M.; Webb, C. J. Versatile *In Situ* Powder X-ray Diffraction Cells for Solid–Gas Investigations. *J. Appl. Crystallogr.* **2010,** *43*, 1456–1463.
36. Adelhelm, P.; Gao, J.; Verkuijlen, M. H. W.; Rongeat, C.; Herrich, M.; van Bentum, P. J. M.; Gutfleisch, O.; Kentgens, A. P. M.; de Jong, K. P.; de Jongh, P. E. Comprehensive Study of Melt Infiltration for the Synthesis of $NaAlH_4$/C Nanocomposites. *Chem. Mater.* **2010,** *22*, 2233–2238.
37. Li, J.; Wang, X.; Huang, Q.; Gamboa, S.; Sebastian, P. J. Studies on Preparation and Performances of Carbon Aerogel Electrodes for the Application of Supercapacitor. *J. Power Sources* **2006,** *158*, 784–788.
38. Al-Muhtaseb, S. A.; Ritter, J. A. Preparation and Properties of Resorcinol-Formaldehyde Organic and Carbon Gels. *Adv. Mater.* **2003,** *15*, 101–114.
39. Bogdanovic, B.; Felderhoff, M.; Germann, M.; Hartel, M.; Pommerin, A.; Schüth, F.; Weidenthaler, C.; Zibrowius, B. Investigation of Hydrogen Discharging and Recharging Processes of Ti-Doped $NaAlH_4$ by X-ray Diffraction Analysis (XRD) and Solid-State NMR Spectroscopy. *J. Alloys Compd.* **2003,** *350*, 246–255.
40. Kellberg, L.; Bildsøe, H.; Jakobsen, H. J. Determination of ^{27}Al Quadrupolar Coupling Parameters and of Metallic Aluminum in Commercial Lithium Aluminum-Hydride by ^{27}Al MAS NMR. *J. Chem. Soc., Chem. Commun.* **1990,** 1294–1295.

41. Adelhelm, P.; de Jong, K. P.; de Jongh, P. E. How Intimate Contact with Nanoporous Carbon Benefits the Reversible Hydrogen Desorption from NaH and NaAlH4. *Chem. Commun.* **2009,** 6261–6263.
42. Brinks, H. W.; Jensen, C. M.; Srinivasan, S. S.; Hauback, B. C.; Blanchard, D.; Murphy, K. Synchrotron X-ray and Neutron Diffraction Studies of $NaAlH_4$ Containing Ti Additives. *J. Alloys Compd.* **2004,** *376*, 215–221.
43. Pitt, M. P.; Vullum, P. E.; Sørby, M. H.; Sulic, M. P.; Jensen, C. M.; Walmsley, J. C.; Holmestad, R.; Hauback, B. C. Structural Properties of the Nanoscopic $Al_{85}Ti_{15}$ Solid Solution Observed in the Hydrogen-Cycled $NaAlH_4$+0.1$TiCl_3$ System. *Acta Mater.* **2008,** *56*, 4691–4701.
44. Bogdanovic, B.; Felderhoff, M.; Kaskel, S.; Pommerin, A.; Schlichte, K.; Schüth, F. Improved Hydrogen Storage Properties of Ti-Doped Sodium Alanate Using Titanium Nanoparticles as Doping Agents. *Adv. Mater.* **2003,** *15*, 1012–1015.
45. Tian, H. Y.; Buckley, C. E.; Paskevicius, M.; Wang, S. B. Carbon Aerogels from Acetic Acid Catalysed Resorcinol-Furfural Using Supercritical Drying for Hydrogen Storage. *J. Supercrit. Fluids* **2011,** *55*, 1115–1117.